

Analytical theory of modulated magnetic solitons

L. D. Bookman* and M. A. Hofer†

Department of Mathematics, North Carolina State University, Raleigh, North Carolina 27695, USA

Droplet solitons are coherently precessing solitary waves that have been recently realized in thin ferromagnets with perpendicular anisotropy. In the strongly nonlinear regime, droplets can be well approximated by a slowly precessing, circular domain wall with a hyperbolic tangent form. Utilizing this representation, this work develops a general droplet modulation theory and applies it to study the long range effects of the magnetostatic field and a nanocontact spin torque oscillator (NC-STO) where spin polarized currents act as a gain source to counteract magnetic damping. An analysis of the dynamical equations for the droplet's center, frequency, and phase demonstrates a negative precessional frequency shift due to long range dipolar interactions, dependent on film thickness. Further analysis also demonstrates the onset of a saddle-node bifurcation at the minimum sustaining current for the NC-STO. The basin of attraction associated with the stable node demonstrates that spin torque enacts a restoring force to excursions of the droplet from the nanocontact center, observed previously in numerical simulations. Large excursions lead to the droplet's eventual decay into spin waves.

I. INTRODUCTION

Magnetic materials are a rich setting for the study of nonlinear, coherent structures. Previously, magnetic excitation mechanisms were predominantly limited to the application of magnetic fields. Nowadays, spin polarized currents^{1,2} are commonly used to create, manipulate, and control nano-scale magnetic excitations such as domain walls³ and vortices⁴, promising candidates for applications^{5,6}. Recently, a strongly nonlinear, coherently precessing localized mode termed a droplet soliton was observed in a nanocontact spin torque oscillator (NC-STO) with perpendicular magnetic anisotropy⁷. The observed droplet exhibited a number of intriguing features including sub-ferromagnetic resonance frequencies, low frequency modulations, and an almost complete reversal of the magnetization within its core, hence a perimeter precession angle of 180 degrees. Supporting micromagnetic simulations demonstrated that the low frequency modulations could be due to an oscillation of the droplet within the nanocontact resulting from some restoring force. Previous theoretical studies of the NC-STO droplet neglected long range dipolar interactions and observed a drift instability whereby the droplet was ejected from the nanocontact⁸. Motivated by these observations, we analytically and numerically study general modulations of a large amplitude magnetic droplet soliton's precessional frequency, phase, and position with particular emphasis on the effects due to magnetostatics, magnetic damping, and spin torque in the nanocontact geometry.

Basic properties of unperturbed, conservative droplets have been extensively studied⁹. A central assumption is that of symmetry which gives rise to conserved quantities and a family of soliton solutions. A stationary droplet soliton can be parameterized by its center, initial phase and precession frequency. In physical problems of interest, these high symmetry, idealized conditions are typically not met. Nevertheless, due to their robust qualities, localized structures may persist. In the context of weak,

symmetry breaking perturbations, a modulation theory can be developed whereby the soliton's parameters are allowed to vary adiabatically in time¹⁰. The resulting soliton modulation equations are analogous to Thiele's equation¹¹ for the motion of a magnetic domain or vortex. One symmetry breaking example is the dissipative droplet soliton, excited in the spin-transfer torque (STT) driven NC-STO where translational invariance and time reversal symmetry are broken⁸. This is precisely the soliton observed in the previously discussed experiment⁷. In steady state, the balance between STT forcing and damping centers the droplet within the nanocontact and selects a specific frequency but the phase is still arbitrary. Modulation theory generalizes the steady state conditions by allowing for slow temporal variations of the conservative droplet's parameters due to the symmetry breaking perturbations. In effect, the droplet is treated as a slowly moving, precessing dipole particle.

In order to make analytical progress tractable and to enable efficient micromagnetic simulations, magnetic soliton studies often neglect the long range component of the magnetostatic field, inherent in any magnetic sample that exhibits a nonuniform magnetization distribution. This is a reasonable approximation in the case of very thin, extended magnetic films¹² where the magnetostatic field takes the local form $-M_z \mathbf{z}$ (M_z is the component of the magnetization perpendicular to the film); however, thickness-dependent, long range corrections can be important¹³. These corrections lead to a breaking of phase invariance¹⁴.

Here, we present the stationary droplet soliton modulation equations for symmetry breaking perturbations. An approximate, analytical representation of the conservative droplet in the strongly nonlinear regime is discussed and used to greatly simplify the modulation equations. The effects of the long range magnetostatic field, a NC-STO, and magnetic damping are studied in detail by a dynamical systems analysis of the modulation equations. The long range component of the magnetostatic field is shown to give rise to a thickness-dependent, neg-

ative precessional frequency shift of the droplet. These dynamics are independent of and do not alter the effects due to the NC-STO and damping. The dissipative droplet soliton is identified as the stable node of a saddle-node bifurcation for sufficiently large spin torque. Consequently, spin torque provides a restoring force to deviations in droplet frequency and position from the nanocontact center. This analytical prediction explains the micromagnetic observation of a restoring force and the corresponding slow droplet modulations observed in Ref. 7. However, large deviations can lead to decay to small amplitude spin waves, helping to explain the previously observed droplet drift instability⁸.

II. MODEL EQUATION AND NONDIMENSIONALIZATION

The mathematical model considered here is the following torque equation for the vector field magnetization \mathbf{M}

$$\begin{aligned} \frac{\partial \mathbf{M}}{\partial t} &= -|\gamma| \mu_0 \mathbf{M} \times \mathbf{H}_{\text{eff}} + \mathbf{P}, \\ \mathbf{H}_{\text{eff}} &= \frac{2A}{\mu_0 M_s^2} \nabla^2 \mathbf{M} + \left(H_0 + \frac{2K_u}{\mu_0 M_s^2} M_z \right) \mathbf{z} + \mathbf{H}_m. \end{aligned} \quad (1)$$

The ferromagnetic material is taken to be of infinite extent in the x - y directions and of finite thickness δ in z . The parameters are the gyromagnetic ratio γ , the permeability of free space μ_0 , the exchange stiffness parameter A , the perpendicular magnetic field amplitude H_0 , the crystalline anisotropy constant K_u , and the saturation magnetization M_s . \mathbf{P} represents any perturbation that maintains the magnetization's total length, i.e. $\mathbf{P} \cdot \mathbf{M} \equiv 0$. The boundary conditions are $\lim_{x^2+y^2 \rightarrow \infty} \mathbf{M} = M_s \mathbf{z}$ and $\partial \mathbf{M} / \partial z = 0$ when $z = \pm \delta / 2$. \mathbf{H}_m is the magnetostatic field resulting from Maxwell's equations.

As derived in Ref. 13, the magnetostatic energy for a z independent magnetization can be given in Fourier space as

$$\begin{aligned} \mathcal{E}_m &= \frac{\delta}{2} \int_{\mathbb{R}^2} \left\{ \frac{|\mathbf{k} \cdot \widehat{\mathbf{M}}_{\perp}|^2}{k^2} [1 - \widehat{\Gamma}(k\delta)] \right. \\ &\quad \left. + |M_z - M_s|^2 \widehat{\Gamma}(k\delta) \right\} d\mathbf{k}, \end{aligned} \quad (2)$$

where

$$\widehat{\Gamma}(\kappa) = \frac{1 - e^{-\kappa}}{\kappa}. \quad (3)$$

Computing the negative variational derivative of \mathcal{E}_m with respect to \mathbf{M} and expanding $\widehat{\Gamma}(k\delta)$ for $|k\delta| \ll 1$ yields the two-dimensional (2D), film thickness averaged magnetostatic asymptotic approximation

$$\begin{aligned} \mathbf{H}_m &\sim -M_z \mathbf{z} + \frac{\delta}{2} \mathbf{H}_{\text{nl}}, \\ \mathbf{H}_{\text{nl}} &= \mathbf{z} \sqrt{-\nabla^2} (M_z - M_s) + \frac{1}{\sqrt{-\nabla^2}} \nabla (\nabla \cdot \mathbf{M}_{\perp}). \end{aligned} \quad (4)$$

The magnetostatic field is composed of the usual local term $-M_z \mathbf{z}$ and a long range, nonlocal contribution $\frac{\delta}{2} \mathbf{H}_{\text{nl}}$. We define $\mathbf{M}_{\perp} = (M_x, M_y)$ and assume δ to be small relative to the typical transverse wavelength of excitation, i.e., the exchange length $l_{\text{ex}} = \sqrt{2A/(\mu M_s^2)}$. The operators are interpreted in Fourier space, e.g., $\sqrt{-\nabla^2} f = |\mathbf{k}| \widehat{f}$ and $\widehat{f}(\mathbf{k})$ is the two-dimensional Fourier transform of f at wavevector \mathbf{k} . Long range magnetostatic corrections have also been used to study domain patterns and vortices in materials with easy-plane anisotropy¹⁵. In order to nondimensionalize the equation, we introduce the dimensionless quality factor $Q = 2K_u/(\mu_0 M_s^2)$ that measures the strength of the uniaxial, crystalline anisotropy. The quality factor is assumed to be greater than unity in order to guarantee the existence of droplet solutions in the unperturbed ($\mathbf{P} = 0, \delta = 0$) problem⁹. Nondimensionalizing time by $[|\gamma| \mu_0 M_s (Q - 1)]^{-1}$, lengths by $l_{\text{ex}} / \sqrt{Q - 1}$, fields by $M_s (Q - 1)$, and setting $\mathbf{m} = \mathbf{M} / M_s$, eq. (1) becomes the 2D model

$$\begin{aligned} \frac{\partial \mathbf{m}}{\partial t} &= -\mathbf{m} \times (\nabla^2 \mathbf{m} + (m_z + h_0) \mathbf{z}) + \mathbf{p}, \\ \mathbf{p} &= \frac{\mathbf{P}}{|\gamma| \mu_0 M_s^2 (Q - 1)} - \frac{\delta}{2} \mathbf{m} \times \mathbf{h}_{\text{nl}}, \quad (x, y) \in \mathbb{R}^2. \end{aligned} \quad (5)$$

Small amplitude, spin wave excitations to the uniform state $\mathbf{m} = \mathbf{z}$ of the unperturbed problem $\mathbf{p} = 0$ admit the exchange dispersion relation $\omega(\mathbf{k}) = 1 + k^2$ where $\omega(0) = 1$ represents the scaled ferromagnetic resonance frequency. The rest of this work concerns soliton dynamics associated with eq. (5).

III. APPROXIMATE DROPLET SOLUTION

First we consider droplet soliton solutions of eq. (5) when $\mathbf{p} = 0$ representing an infinitely thin, undamped ferromagnet with strong perpendicular, uniaxial anisotropy. It is convenient to represent \mathbf{m} in spherical coordinates by the radial unit vector, $\mathbf{m} = [\cos \Phi \sin \Theta, \sin \Phi \sin \Theta, \cos \Theta]$. In these coordinates, the stationary droplet soliton solution to eq. (5) is the positive, monotonically decaying solution of the boundary value problem

$$\begin{cases} -\left(\frac{d^2}{d\rho^2} + \frac{1}{\rho} \frac{d}{d\rho} \right) \Theta_0 + \sin \Theta_0 \cos \Theta_0 - \omega \sin \Theta_0 = 0, \\ \frac{d\Theta_0}{d\rho}(\mathbf{x}_0; \omega) = 0, & \lim_{\rho \rightarrow \infty} \Theta_0(\rho; \omega) = 0, \end{cases} \quad (6)$$

where $\Theta = \Theta_0$, $\Phi = (\omega + h_0)t + \Phi_0$, ρ is the radial distance from \mathbf{x}_0 , and $0 < \omega < 1$ ⁹. Consequently, the stationary droplet is parameterized by frequency ω , the initial phase Φ_0 , and the initial droplet center coordinates \mathbf{x}_0 , the latter generated by invariances with respect to azimuthal rotations of \mathbf{m} and translations. Droplets can also be made to propagate¹⁶. While this work is concerned with

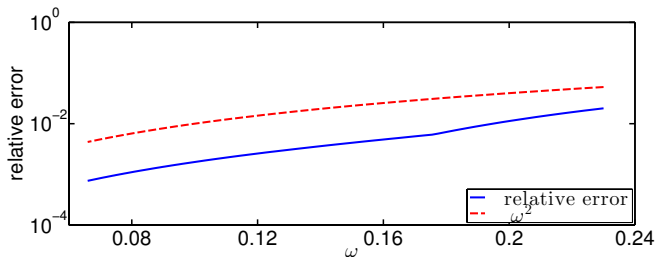


FIG. 1: Relative difference between approximate and numerically computed droplets (solid). ω^2 (dashed) for comparison of convergence order.

stationary droplets, we will use the propagating solution in the Appendix to implement the modulation theory. The boundary conditions in (6) arise from the far field decay condition applied to (1) and the requirement that (6) remain finite near the droplet center.

In the small ω regime, the droplet profile takes the approximate form^{17,18}

$$\cos \Theta_0 = \tanh(\rho - 1/\omega), \quad 0 < \omega \ll 1. \quad (7)$$

We have derived this approximate solution using singular perturbation theory (Appendix A) and find it to be accurate to $\mathcal{O}(\omega^2)$ and uniformly valid for all $\rho \in (0, \infty)$. The error in the approximate solution (7) is shown in Fig. 1. Based on the form of the solution (7), the small ω droplet takes the form of a slowly precessing (absent the applied field), circular domain wall with radius $1/\omega$. Expanding this approximate solution for the droplet around $\rho = 0$, we observe $\Theta_0(0) = \pi$ to all orders in ω . However, the magnetization at the center of the small ω droplet cannot equal $-\mathbf{z}$, due to its nontopological structure⁹. For the rest of this work, we will consider the small ω regime and use the approximate form (7) for the droplet.

IV. MODULATION EQUATIONS

We now consider the effects of small symmetry breaking perturbations \mathbf{p} in eq. (5) on the droplet (7). The perturbation has spherical components $p_\Theta = \mathbf{p} \cdot \Theta$ and $p_\Phi = \mathbf{p} \cdot \Phi$. The principle effects can be captured by allowing the droplet's parameters to vary adiabatically in time, e.g., $\omega = \omega(t)$ with $|d\omega/dt| \ll 1$. The method of multiple scales allows for the determination of their evolution. Following the approach in Ref. 19 developed for perturbations to a Nonlinear Schrödinger soliton, we linearize eq. (5) around a droplet and apply solvability conditions at $\mathcal{O}(|\mathbf{p}|)$ to determine the modulation equa-

tions (Appendix B),

$$\frac{d\omega}{dt} = -\frac{\omega^3}{4\pi} \int_{\mathbb{R}^2} \text{sech}(\rho - 1/\omega) p_\Theta \, d\mathbf{x}, \quad (8)$$

$$0 = \int_{\mathbb{R}^2} \text{sech}(\rho - 1/\omega) p_\Phi \begin{pmatrix} \cos \varphi \\ \sin \varphi \end{pmatrix} \, d\mathbf{x}, \quad (9)$$

$$\frac{d\Phi_0}{dt} = \frac{\omega}{4\pi} \int_{\mathbb{R}^2} \text{sech}(\rho - 1/\omega) p_\Phi \, d\mathbf{x}, \quad (10)$$

$$\frac{d\mathbf{x}_0}{dt} = \frac{\omega}{2\pi} \int_{\mathbb{R}^2} \text{sech}(\rho - 1/\omega) p_\Theta \begin{pmatrix} \cos \varphi \\ \sin \varphi \end{pmatrix} \, d\mathbf{x}, \quad (11)$$

where the perturbation (p_Θ, p_Φ) is evaluated at the droplet solution (7) and (ρ, φ) are the polar coordinates for the domain \mathbb{R}^2 . Note that eq. (9) is not an evolution equation, but rather serves as a constraint on admissible perturbations. When this constraint is not satisfied, a nonzero momentum can be generated and the droplet no longer remains stationary. The stationary assumption is essential not only to the modulation equations themselves but also to the small ω approximation given in eq. (7) and therefore a different set of modulation equations is required for the non-stationary case. For example, a magnetic field gradient will accelerate a stationary droplet²⁰.

A. Long Range Magnetostatic Perturbation

We now investigate specific perturbations of physical relevance. First, the long range magnetostatic field is considered. After applying modulation theory, we find that the contribution to eqs. (8)-(11) takes the form

$$p_\Theta = 0, \quad p_\Phi = -\delta \sin \Theta_0 \sqrt{-\nabla^2} (1 - \cos \Theta_0) / 2. \quad (12)$$

Consequently, thickness dependent magnetostatic effects only enter in eqs. (9) and (10). The constraint equation (9) is automatically satisfied because p_Φ depends only on ρ so the φ integrals vanish. What is left is the expression for the slowly varying phase Φ_0 . Evaluating (10) with (12) represents a precessional frequency shift of the droplet

$$\frac{d\Phi_0}{dt} = -\frac{\delta\omega}{4} \int_0^\infty \text{sech}^2(\rho - 1/\omega) \times \{ \sqrt{-\nabla^2} [1 - \tanh(\rho - 1/\omega)] \} \rho \, d\rho. \quad (13)$$

The total droplet frequency is $h_0 + \omega + \Phi'_0$. Since the integrand is strictly positive for $\rho \in (0, \infty)$, eq. (13) represents a negative frequency shift which is plotted in Fig. 2 as a function of ω . Micromagnetic simulations (Appendix C) yield good, asymptotic $\mathcal{O}(\delta\omega)$ agreement as expected.

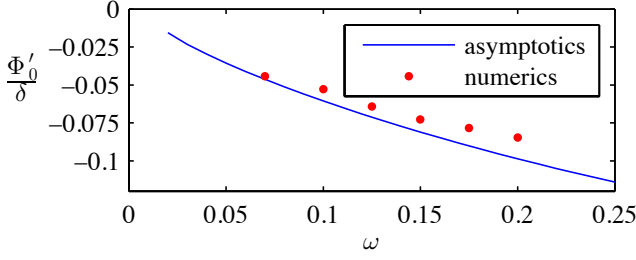


FIG. 2: Negative frequency shift due to long range, thickness dependent magnetostatic corrections. Equation (13) (solid) and micromagnetic simulations with $\delta = 0.1$ (dots).

B. NC-STO and Damping Perturbations

We now consider the effects of damping and STT. A NC-STO consists of two magnetic layers, one that is assumed fixed and acts as a spin polarizer of the driving current. The other layer is dynamic, resulting from the solution of eq. (5). When the polarizing layer is \mathbf{z} , the perturbation \mathbf{p} takes the form⁸

$$p_\Theta = -\alpha\omega \sin \Theta_0 + \sigma V(\rho_\star - \rho) \frac{\sin \Theta_0}{1 + \nu \cos \Theta_0}, \quad p_\Phi = 0, \quad (14)$$

where α is the damping coefficient, $\nu = (\lambda_{\text{st}}^2 - 1)/(\lambda_{\text{st}}^2 + 1)$, $\lambda_{\text{st}} \geq 1$ is the spin torque asymmetry, ρ_\star is the nanocontact radius, and V is a localized function. In the following analysis we take V to be the Heaviside step function thus defining the region of spin polarized current flow as a disk with radius ρ_\star . The STT coefficient $\sigma = I/I_0$ is proportional to the applied, dc current I with nondimensionalization $I_0 = (\lambda_{\text{st}}^2 + 1)M_s^2 e \mu_0 \pi \rho_\star^2 \delta / (\hbar \epsilon \lambda_{\text{st}}^2)$ where ϵ is the spin-torque polarization, e is the electron charge, and \hbar is the modified Planck's constant. For simplicity, we take $\lambda_{\text{st}} = 1$, i.e., no asymmetry. Both α and σ are assumed small, but as a balance must be maintained for the sustenance of a dissipative soliton⁸, they are of the same order. Substituting this perturbation into (8)–(11), we arrive at a system of three ordinary differential equations (ODEs). Since rotational symmetry is not broken for a circular nanocontact, we are free to rotate the plane and thereby eliminate one of the two equations for the center. The modulation system is thus

$$\begin{aligned} \frac{d\omega}{dt} &= \alpha\omega^2(\omega + h_0) \\ &\quad - \frac{\sigma\omega^3}{4\pi} \int_{|\mathbf{x}| < \rho_\star} \text{sech}^2(|\mathbf{x} - \mathbf{x}_0| - 1/\omega) d\mathbf{x} \\ \frac{dx_0}{dt} &= - \frac{\sigma\omega^3}{2\pi} \int_{|\mathbf{x}| < \rho_\star} \text{sech}^2(|\mathbf{x} - \mathbf{x}_0| - 1/\omega) \frac{x - x_0}{|\mathbf{x} - \mathbf{x}_0|} d\mathbf{x}. \end{aligned} \quad (15)$$

Note that when $h_0 = 0$ and $\sigma = 0$, the remaining ODE $\omega' = \alpha\omega^3$ agrees with the result in Ref. 21 and the

more general result for solitons of non-trivial topological charge in Ref. 22. Equations (15) and (16) do not depend upon the slowly varying phase Φ_0 so that the inclusion of long range magnetostatic effects will lead to the same frequency shift given in eq. (13), decoupling from the ODEs (15) and (16). The fixed points of this system correspond to steady state conditions where there is a balance between uniform damping and localized spin torque, i.e., a dissipative droplet soliton. A fixed point at $(\omega, x_0) = (\omega_\star, 0)$ leads to a relationship between the sustaining current and precession frequency

$$\frac{\sigma}{\alpha} = \frac{2(\omega_\star + h_0)}{1 + \omega_\star \log[\text{sech}(\rho_\star - \frac{1}{\omega_\star})/2] + \rho_\star \tanh(\rho_\star - \frac{1}{\omega_\star})}. \quad (17)$$

Linearizing about the fixed point, we find the eigenvalues

$$\lambda_1 = \frac{1}{2}\omega_\star [\sigma \tanh(\rho_\star - 1/\omega_\star) + \sigma - \rho_\star \sigma \text{sech}^2(\rho_\star - 1/\omega_\star) - 2\alpha h_0], \quad (18)$$

$$\lambda_2 = -\frac{1}{2}\rho_\star \sigma \omega_\star \text{sech}^2(\rho_\star - 1/\omega_\star). \quad (19)$$

For physical parameters, λ_2 is always negative, however λ_1 can change sign as ω_\star is varied and hence the stability of the fixed point can change. This family of fixed points arises from a saddle-node bifurcation occurring as the current is increased through the minimum sustaining current (Fig. 3(a-d)). The lower, stable branch of this saddle node bifurcation is the dissipative soliton. Figure 3(a) shows that the frequency changes little as the sustaining current is increased from its minimum, stable value. To a good approximation, the frequency is $\omega_\star = 1/\rho_\star$, as illustrated by the horizontal line in Fig. 3(a). Expanding (17) for ω_\star close to $1/\rho_\star$, on the stable branch, the fixed point relation can be simplified to

$$\frac{\sigma}{\alpha} \sim \frac{2(h_0 + \omega_\star)}{1 + \rho_\star(\rho_\star - 1/\omega_\star)}, \quad |\rho_\star - 1/\omega_\star| \ll 1. \quad (20)$$

While this relation gives good agreement in the vicinity of the stable fixed points, it does not predict the minimum sustaining current. Evaluating λ_1 for σ given by (20) and expanding for $0 < \rho_\star - 1/\omega_\star \ll 1$, the eigenvalue λ_1 in (18) is found to be negative, hence the branch of (17) nearest to $\omega_\star = 1/\rho_\star$ is indeed stable. The stable branch is further verified by micromagnetic simulations (Appendix C) shown in Fig. 3(a).

Interestingly, the dissipative soliton is not a global attractor. The saddle point's stable manifold (solid curve in Fig. 3(c-d)) denotes the upper boundary in phase space of the basin of attraction for the dissipative soliton. A droplet with frequency ω and position x_0 lying within the basin of attraction will generally increase in frequency, move toward the nanocontact center, then decrease in frequency to ω_\star , converging to the dissipative soliton fixed point. If an initial droplet lies outside the basin of attraction, the frequency will increase, causing the droplet to decrease in amplitude. An analysis of the small to moderate amplitude regime²⁰ shows that the soliton decays to spin waves as its frequency approaches the ferromagnetic resonance frequency $\omega \rightarrow 1$. Figures 3(b)-(d)

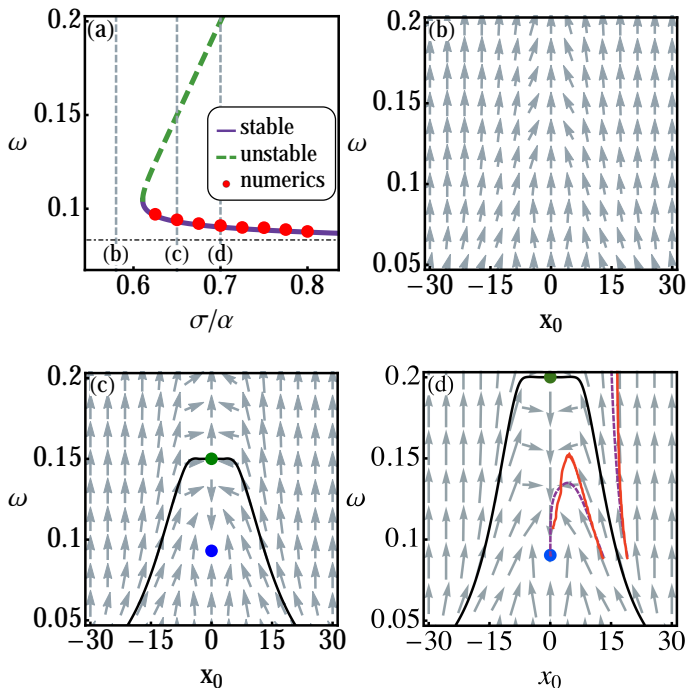


FIG. 3: (a) Dissipative soliton relation (17). Horizontal line is $\omega = 1/\rho_*$. (b-d) ODE vector fields corresponding to equations (15), (16) as σ varies (b) just before the saddle-node bifurcation (c), just after and (d) far past bifurcation. The upper/lower dot corresponds to the unstable/stable fixed point. The solid black curve encloses the basin of attraction. Parameters are $\rho_* = 12$, $h_0 = 0.5$, and $\alpha = 0.01$. (d) includes trajectories from ODE theory (dashed) and micromagnetics (solid).

show the vector field of this system before and after the saddle node bifurcation. Figure 3(d) depicts trajectories (dashed) generated by numerical evolution of eqs. (15) and (16) with the initial conditions $(\omega_*, 13)$ and $(\omega_*, 20)$. The solid curves result from full micromagnetic simulations with the same initial conditions. These numerical experiments show good agreement up to evolution times $\mathcal{O}(\alpha^{-2})$, as expected for this approximate theory. The resulting discrepancies lead to modulation theory slightly over-predicting the radius of the basin of attraction compared to what is observed from micromagnetics.

The other physical parameters in the fixed point relation (17) are h_0 and ρ_* . Based on the analytical form of eq. (17), h_0 should shift resulting stability curve. Near the stable branch, the denominator of eq. (20) is $\mathcal{O}(1)$ hence an shift of $\mathcal{O}(h_0)$ is expected. Numerical experiments with eq. (17) suggest that changes in h_0 do essentially serve to shift the minimum sustaining current by a constant (close to h_0). This is apparent from the numerical results shown in Figs. 4 and 5. Figure 6 depicts the basin of attraction radius ρ_b (the value of x_0 at the edge of the basin of attraction when $\omega = \omega_*$) scaled by ρ_* . As

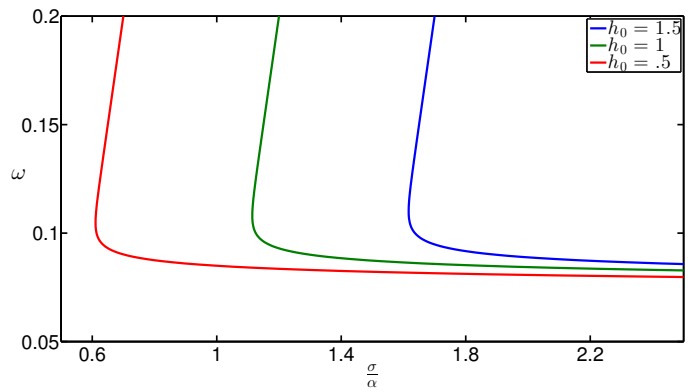


FIG. 4: Fixed points, both stable and unstable for several values of h_0 . The primary effect of h_0 is to shift these curves of fixed points along the σ/α axis.

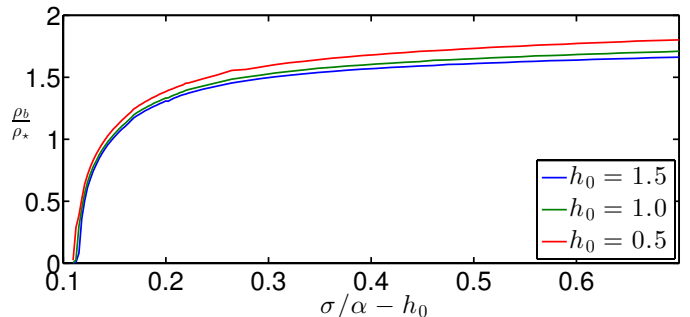


FIG. 5: Scaled radius of the basin of attraction ρ_b/ρ_* at $\omega = \omega_*$ with $\rho_* = 12$. While the center of the basin of attraction depends on h_0 , the width of the basin remains essentially unchanged as h_0 varies.

the current is increased, the basin radius rapidly exceeds $\frac{3}{2}\rho_*$ so that a droplet placed well outside the nanocontact may still experience a restoring force to the nanoncontact center.

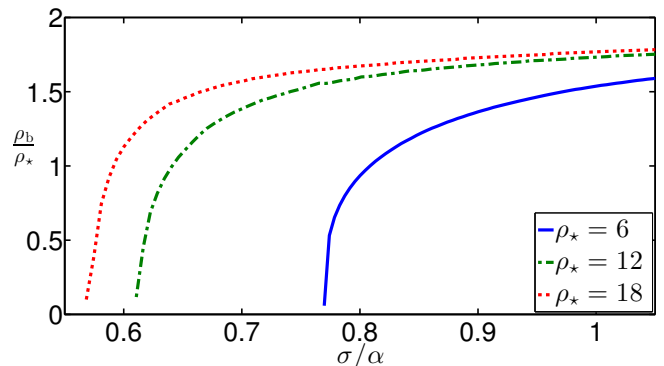


FIG. 6: Basin of attraction radius, ρ_b at $\omega = \omega_*$ scaled by nanocontact radius, ρ_* . Applied field is $h_0 = 0.5$.

V. DISCUSSION

We now describe some physical and theoretical implications of the presented analysis.

The modulation equations (8)-(11) are the droplet soliton analogue of Thiele's equation for magnetic vortices. They treat the droplet as a precessing dipole, describing adiabatic changes in its precessional frequency, phase, and center due to symmetry breaking perturbations. This description is valid so long as the evolution times satisfy $t \ll \epsilon^{-2}$ where ϵ characterizes the magnitude of the perturbation $\mathbf{p} = \mathcal{O}(\epsilon)$. Breaking of the constraint eq. (9) can lead to an acceleration of the droplet so that a more general modulation description of propagating droplets would be required in this case. Finally, we have neglected coupling to radiation modes in this analysis which is, for example, important in the small amplitude regime of NC-STOs¹.

It is important to point out that the negative frequency shift due to long range magnetostatic effects is independent of and does not influence the results pertaining to NC-STO and damping perturbations. Recalling that $0 < \omega < 1$, stationary droplets in the absence of long range magnetostatics and applied field are always dynamic. The negative frequency shift suggests that a droplet in a sufficiently thick film could be static, which would correspond to a magnetic bubble²³. However, this regime is strictly outside the validity range of the asymptotic expression (13) so it is likely that a non-perturbative analysis is required for further investigation.

Micromagnetic simulations and experimentally observed low frequency modulations in Ref. 7 suggest the existence of a restoring force due to the NC-STO. Our analysis presented here precisely describes how this restoring force arises, as the manifestation of a stable fixed point and its basin of attraction. That the dissipative soliton in the NC-STO is not a global attractor was observed in micromagnetic simulations previously in the form of the drift instability⁸. As it is known that a magnetic field gradient can accelerate a stationary droplet²⁰, we postulate that STT provides a restoring force that can keep the droplet inside the nanocontact for a sufficiently small gradient. These competing effects could also account for the observed shift of the droplet with respect to the NC-STO center when Oersted fields are included in the model. However, a sufficiently strong field gradient that overcomes the STT restoring force can lead to expulsion of the droplet, hence a drift instability. Because a field gradient perturbation does not maintain the constraint (9), further investigation of this requires the study of modulated propagating droplets in the presence of an NC-STO.

An additional experimental implication of our results is that of a restricted regime of droplet soliton excitation. In NC-STOs, droplets can be nucleated by a spin wave instability (subcritical Hopf bifurcation) associated with the uniform state $\mathbf{m} = \mathbf{z}$ ⁸. However, the instability may not generate an excitation that lies within the droplet

soliton basin of attraction. Furthermore, Fig. 4 shows that a large applied field shifts the minimum sustaining current to higher values. Since the spin wave instability only weakly depends on the applied field^{1,8}, a sufficiently large field may shift the stable dissipative soliton branch above a given applied current so that the droplet is no longer nucleated in a NC-STO.

VI. CONCLUSION

Using singular perturbation theory we have derived modulation equations for parameters of a droplet soliton under very general perturbations. This theory was applied to two such physically relevant perturbations: 1) higher-order, long range effects of the magnetostatic field and 2) damping and spin transfer torque forcing in a nanocontact spin torque oscillator. The key result is that these long range effects result in a down shift of the overall droplet frequency. For a NC-STO system, we predict that a droplet shifted from the nanocontact center can be drawn back by a STT-induced restoring force. Sufficiently large shifts cause damping to overwhelm STT effects so that the droplet soliton is no longer an attractor, hence decays into spin waves. For both perturbations investigated we see good agreement between micromagnetic simulations and the reduced order models proposed here. The robustness of magnetic droplet solitons to symmetry breaking perturbations we have demonstrated here suggests that their initial observation in Ref. 7 represents the beginning of a rich inquiry into novel nonlinear physics.

Appendix A: Approximate Droplet Calculation

Here we offer more detail on the derivation of the small ω solution to (6). For a similar derivation, see Ref. 18. A uniformly valid approximate solution to this problem is sought in the limit $0 < \omega \ll 1$. We begin by introducing a shifted coordinate system $\rho = R + \frac{A}{\omega}$, where A is some constant which will be determined by solvability conditions. In this coordinate, (6) becomes

$$-\left(\frac{d^2}{dR^2} + \frac{1}{(R + \frac{A}{\omega})} \frac{d}{dR}\right) \Theta_0 + \sin \Theta_0 \cos \Theta_0 - \omega \sin \Theta_0 = 0 \quad (\text{A1})$$

Expanding (A1) and keeping terms only to leading order in ω gives

$$-\frac{d^2 \Theta_0}{dR^2} + \sin \Theta_0 \cos \Theta_0 + \omega \left(-\frac{1}{A} \frac{d \Theta_0}{dR} - \sin \Theta_0 \right) = \mathcal{O}(\omega^2). \quad (\text{A2})$$

Inserting the asymptotic expansion $\Theta_0 = \Theta_{0,0} + \omega \Theta_{0,1} + \mathcal{O}(\omega^2)$ into (A2) and equating like terms at each order

in ω we obtain

$$\mathcal{O}(1) : -\frac{d^2\Theta_{0,0}}{dR^2} + \sin\Theta_{0,0}\cos\Theta_{0,0} = 0 \quad (\text{A3})$$

$$\mathcal{O}(\omega) : -\frac{d^2\Theta_{0,1}}{dR^2} + \cos(2\Theta_{0,0})\Theta_{0,1} = \frac{1}{A}\frac{d\Theta_{0,0}}{dR} + \sin\Theta_{0,0}. \quad (\text{A4})$$

It is readily verified that the solution to (A3) is $\Theta_{0,0} = \cos^{-1}(\tanh(R + R_0))$ where R_0 is some arbitrary constant. For simplicity, we choose $R_0 = 0$ since it is not restricted unless we seek a higher order solution. Taking $L = -\frac{d^2}{dR^2} + \cos(2\Theta_{0,0})$, equation (A4) is of the form $L\psi = f$. In this case, L is a Schrödinger operator and hence self-adjoint with kernel spanned by $\text{sech}(R)$. Solvability then requires that the right hand side of eq. (A4)

$$\frac{1}{A}\frac{d\Theta_{0,0}}{dR} + \sin\Theta_{0,0} = \left(1 - \frac{1}{A}\right)\text{sech}(R),$$

is orthogonal to the kernel of L . Thus $(1 - \frac{1}{A})\text{sech}(R)$ will be a nontrivial element of the kernel of L unless $A \equiv 1$. Further, this choice of A means the equation at $\mathcal{O}(\omega)$ is trivially satisfied by taking $\Theta_{0,1} \equiv 0$. Substituting back to the ρ coordinate system, we obtain the leading order solution

$$\Theta_0 = \cos^{-1}\left(\tanh\left(\rho - \frac{1}{\omega}\right)\right) + \mathcal{O}(\omega^2). \quad (\text{A5})$$

This solution is expected to be valid in the regime when R is $\mathcal{O}(1)$, that is when ρ is of the same order as $1/\omega$. The residual of eq. (6) with the approximate solution (A5) is

$$\frac{(1 - \rho\omega)\text{sech}(\rho - \frac{1}{\omega})}{\rho}.$$

Examination of this residual shows that the approximate solution (A5) is in fact uniformly valid for all ρ and introduces deviations at $\mathcal{O}(\omega^2)$.

Appendix B: Modulation Equations Derivation

For this derivation, we rescale the perturbation with a small parameter ϵ , $\mathbf{p} \rightarrow \epsilon\mathbf{p}$, $0 < \epsilon \ll 1$ and introduce the ‘‘slow’’ time $T = \epsilon t$. The modulated droplet takes the asymptotic form

$$\Theta(\mathbf{x}, t) = \Theta_0(\mathbf{x} + \mathbf{x}_0(T); \omega(T)) + \epsilon\Theta_1(\mathbf{x}, t, T) + \dots$$

$$\Phi(\mathbf{x}, t) = \Phi_0(T) + h_0 t + \int_0^t \omega(\epsilon t') dt' + \epsilon \frac{\Phi_1(\mathbf{x}, t, T)}{\sin(\Theta_0)} + \dots,$$

where Θ_0 and $\Phi_0 + h_0 t + \int_0^t \omega(\epsilon t') dt'$ represent the conservative droplet with slowly varying parameters. Introducing these into the perturbed Landau-Lifshitz equation,

at $\mathcal{O}(\epsilon)$ we obtain $\psi_t = L\psi + f$. where

$$L_\Phi = -\nabla^2 + (-\nabla\Theta_0 \cdot \nabla\Theta_0 + \cos^2(\Theta_0) - \omega(T)\cos(\Theta_0)) \quad (\text{B1})$$

$$L_\Theta = -\nabla^2 + \cos(2\Theta_0) - \omega(T)\cos(\Theta_0) \quad (\text{B2})$$

$$\psi = \begin{pmatrix} \Theta_1 \\ \Phi_1 \end{pmatrix} \quad (\text{B3})$$

$$L = \begin{pmatrix} 0 & L_\Phi \\ -L_\Theta & 0 \end{pmatrix} \text{ and} \quad (\text{B4})$$

$$f = \begin{pmatrix} p_\Theta - \Theta_{0,\omega}\frac{d\omega}{dT} - \nabla\Theta_0 \cdot \frac{d\mathbf{x}_0}{dT} \\ p_\Phi - \sin(\Theta_0)\frac{d\Phi_0}{dT} \end{pmatrix} \quad (\text{B5})$$

Since algebraic growth of either Θ_1 or Φ_1 would lead to secularities, we apply the condition that f is orthogonal to the generalized null space of the adjoint of L (L^\dagger), denoted by $N(L^\dagger)$ ¹⁹. By differentiating the leading order problem with respect to each of the soliton parameters, $\mathbf{x}_0 = (x_1, x_2)$, ω , Φ_0 , and $\mathbf{V} = (V_1, V_2)$ (we temporarily allow for moving droplets with velocity \mathbf{V}), and evaluating at the conservative, stationary droplet we obtain

$$N(L^\dagger) = \text{span}\left\{ \begin{pmatrix} 0 \\ \frac{\partial\Theta_0}{\partial x_i} \\ 0 \end{pmatrix}, \begin{pmatrix} \sin(\Theta_0) \\ 0 \end{pmatrix}, \begin{pmatrix} 0 \\ \frac{\partial\Theta_0}{\partial\omega} \\ 0 \end{pmatrix}, \begin{pmatrix} \sin(\Theta_0)\frac{\partial\Phi_0}{\partial V_i} \\ 0 \end{pmatrix} \right\}, \quad i = 1, 2. \quad (\text{B6})$$

The vector $(\frac{\partial\Phi}{\partial V_1}, \frac{\partial\Phi}{\partial V_2})$ is determined according to $(\frac{\partial\Phi}{\partial V_1}, \frac{\partial\Phi}{\partial V_2}) = \tilde{\Phi}(\cos(\varphi), \sin(\varphi))$, where $\tilde{\Phi}$ satisfies the boundary value problem

$$\left\{ \begin{array}{l} -\left(\frac{\partial^2}{\partial\rho^2} + \frac{1}{\rho}\frac{\partial}{\partial\rho} - \frac{1}{\rho^2}\right)\tilde{\Phi} \\ \quad + \left[-\left(\frac{\partial}{\partial\rho}\Theta_0\right)^2 + \cos^2(\Theta_0) - \omega\cos(\Theta_0)\right]\tilde{\Phi} = -\frac{\partial}{\partial\rho}\Theta_0 \\ \lim_{\rho \rightarrow 0}\tilde{\Phi} \text{ is finite,} \quad \lim_{\rho \rightarrow \infty}\tilde{\Phi} = 0. \end{array} \right. \quad (\text{B7})$$

Applying the solvability condition that f is orthogonal to $N(L^\dagger)$ gives

$$\frac{d\omega}{dT} = \frac{1}{\frac{\partial\mathcal{N}}{\partial\omega}} \int_{\mathbb{R}^n} \sin(\Theta_0)p_\Theta d\mathbf{x} \quad (\text{B8})$$

$$0 = \int_{\mathbb{R}^n} \nabla\Theta_0 p_\Phi d\mathbf{x} \quad (\text{B9})$$

$$\frac{d\Phi_0}{dT} = \frac{1}{\frac{\partial\mathcal{N}}{\partial\omega}} \int_{\mathbb{R}^n} \frac{\partial\Theta_0}{\partial\omega} p_\Phi d\mathbf{x} \quad (\text{B10})$$

$$\frac{d\mathbf{x}_0}{dT} = \frac{1}{\pi \int_0^\infty \tilde{\Phi} \frac{\partial\Theta_0}{\partial\rho} \rho d\rho} \int_{\mathbb{R}^n} \sin(\Theta_0) \begin{pmatrix} \cos(\varphi) \\ \sin(\varphi) \end{pmatrix} \tilde{\Phi} p_\Theta d\mathbf{x}. \quad (\text{B11})$$

where $\mathcal{N} = \int_{\mathbb{R}^2} (1 - \cos(\theta)) d\mathbf{x}$ is the total spin. Substituting in the small ω solution gives equations (8)-(11).

Appendix C: Numerical Methods

Micromagnetic simulations were performed using a pseudospectral/Fourier discretization in space and a method of lines in time similar to those presented in previous work⁸. The spatial domain was taken to be square, typically $[-75, 75] \times [-75, 75]$, large enough that the solution decayed to zero at the boundary. The mesh width was taken small enough to provide sufficient decay of the fourier coefficients of the solution, typically $\Delta x = \Delta y = 0.4$. To improve convergence properties of this method, the region associated with the nanocontact was smoothed and approximated by a hyper-gaussian $\exp(-z^8)$, normalized so that the total current density is the same as for flow in a cylinder with sharp edges. For simulations involving the magnetostatic correction, the nonlocal terms were implemented in fourier space.

The time evolution was conducted with an adaptive ex-

plicit Runge-Kutta method, with normalization at each time step to preserve unit length of the magnetization vector. Initial conditions were chosen to be the approximate conservative droplet at some frequency generally near the frequency of the fixed point. The precessional frequency of the droplet was obtained by examining a fixed spatial point near the edge of the nanocontact, fitting a line to the time dependence of the in-plane magnetization phase. For a purely precessional mode, the frequency of the droplet is the slope of this line. When ω is changing in time, we utilize the approximate droplet expansion. For the approximate solution it holds that

$$\omega^2 = \frac{\mathcal{N}}{4 \int_{\mathbb{R}^2} (x - x_0)^2 (1 - \cos(\Theta_0)) dx}.$$

This relation was used to extract frequencies from the micromagnetic simulations see in Fig. 3.

* ldbookma@ncsu.edu

† mahoefer@ncsu.edu

¹ J. C. Slonczewski, *J. Magn. Magn. Mater.* **195**, L261 (1999).

² L. Berger, *Phys. Rev. B* **54**, 9353 (1996).

³ O. Boulle, G. Malinowski, and M. Klui, *Mat. Sci. Eng.: R: Rep.* **72**, 159 (2011).

⁴ S. Petit-Watelot, J.-V. Kim, A. Ruotolo, R. M. Otxoa, K. Bouzehouane, J. Grollier, A. Vansteenkiste, B. Van de Wiele, V. Cros, and T. Devolder, *Nat. Phys.* **8**, 682 (2012).

⁵ D. A. Allwood, G. Xiong, C. C. Faulkner, D. Atkinson, D. Petit, and R. P. Cowburn, *Science* **309**, 1688 (2005).

⁶ V. S. Pribiag, I. N. Krivorotov, G. D. Fuchs, P. M. Braganca, O. Ozatay, J. C. Sankey, D. C. Ralph, and R. A. Buhrman, *Nat. Phys.* **3**, 498 (2007).

⁷ S. M. Mohseni, S. Sani, J. Persson, T. A. Nguyen, S. Chung, Y. Pogoryelov, P. Muduli, E. Iacocca, A. Eklund, R. Dumas, *et al.*, *Science* **339**, 1295 (2013).

⁸ M.A. Hoefer, T. J. Silva, and M. W. Keller, *Phys. Rev. B* **82**, 054432 (2010).

⁹ A. M. Kosevich, B. Ivanov, and A. Kovalev, *Phys. Rep.* **194**, 117 (1990).

¹⁰ Y. S. Kivshar and B. A. Malomed, *Rev. Mod. Phys.* **61**, 763 (1989).

¹¹ A. A. Thiele, *Phys. Rev. Lett.* **30**, 230 (1973).

¹² G. Gioia and R. D. James, *Proc. R. Soc. Lond. A* **453**, 213 (1997).

¹³ C. J. Garcia-Cervera, *Eur. J. Appl. Math.* **15**, 451 (2004).

¹⁴ N. Papanicolaou and T. Tomaras, *Nucl. Phys. B* **360**, 425 (1991).

¹⁵ C. J. Garcia-Cervera and W. E., *J. Appl. Phys.* **90**, 370 (2001). R. V. Kohn and V. V. Slastikov, *Proc. Roy. Soc. A* **461**, 143 (2005). J.G. Caputo, Y. Gaididei, V. P. Kravchuk, F. G. Mertens, and D. D. Sheka, *Phys. Rev. B* **76**, 174428 (2007).

¹⁶ M. A. Hoefer and M. Sommacal, *Physica D* **241**, 890 (2012).

¹⁷ A. M. Kosevich, B. A. Ivanov, and A. S. Kovalev, *Sov. Sci. Rev., Sect. A, Phys. Rev.* **6**, 171 (1986).

¹⁸ B. A. Ivanov and V. A. Stephanovich, *Phys. Lett. A* **141**, 89 (1989).

¹⁹ M. I. Weinstein, *SIAM J. Math. Anal.* **16**, 472 (1985).

²⁰ M. A. Hoefer, M. Sommacal, and T. J. Silva, *Phys. Rev. B* **85**, 214433 (2012).

²¹ V. Baryakhtar, B. Ivanov, and A. Sukstanskii, *Physics Letters A* **119**, 191 (1986).

²² V. G Baryakhtar, B. A. Ivanov, A. L. Sukstanskii, and E. Y. Melikhov, *Physical Review B* **56**, 619 (1997).

²³ F. H. D. Leeuw, R. V. D. Doel, and U. Enz, *Rep. Prog. Phys.* **43**, 689 (1980) **43**, 689 (1980).